Three-dimensional multiwaveguide probe array for light delivery to distributed brain circuits

Anthony N. Zorzos,[1,2,3] Jorg Scholvin,[1,2,3] Edward S. Boyden,[1,2,*] and Clifton G. Fonstad[2,3]

[1]*MIT Media Lab and MIT McGovern Institute, Departments of Brain and Cognitive Sciences and Biological Engineering, Massachusetts Institute of Technology, 77 Massachusetts Avenue, Cambridge, Massachusetts 02139, USA*

[2]*MIT Microsystems Technology Laboratory, Massachusetts Institute of Technology, 77 Massachusetts Avenue, Cambridge, Massachusetts 02139, USA*

[3]*MIT Department of Electrical Engineering and Computer Science, Massachusetts Institute of Technology, 77 Massachusetts Avenue, Cambridge, Massachusetts 02139, USA*

**Corresponding author: esb@media.mit.edu*

Received August 3, 2012; revised October 10, 2012; accepted October 18, 2012; posted October 19, 2012 (Doc. ID 173452); published November 20, 2012

To deliver light to the brain for neuroscientific and neuroengineering applications like optogenetics, in which light is used to activate or silence neurons expressing specific photosensitive proteins, optical fibers are commonly used. However, an optical fiber is limited, to delivering light to a single target within the 3D structure of the brain. Here, we describe the design and fabrication of an array of thin microwaveguides, which terminates at a three-dimensionally distributed set of points, appropriate for delivering light to targets distributed in a 3D pattern throughout the brain.

© 2012 Optical Society of America

OCIS codes: 170.0170, 130.2755, 130.3120, 130.3990, 230.3990, 230.7370.

The ability to deliver light into the brain for the purpose of controlling neural activity or other biological processes has opened up new frontiers in both basic neuroscience and neuroengineering. One arena of great activity is in the use of microbial opsins [1–5] to make neurons activatable or silenceable by light. To date, numerous *in vivo* studies have used optical fibers and LEDs [6–9] to deliver visible light into brain targets in which neurons express opsins, but the complex nature of brain circuits demands a technology that can address complex-shaped, distributed neural circuits. We recently developed a linear probe comrising a set of integrated microwaveguides running in parallel to each other, microfabricated on a single substrate, and capable of delivering light independently to multiple brain targets along the probe axis [10]. We now extend this design to the case of 3D light delivery to a set of targets distributed throughout the brain, by first fabricating waveguide combs containing many linear probes parallel to one another, then aligning multiple combs in a custom-engineered baseplate.

Each 3D probe is composed of three microfabricated elements: a set of waveguide combs, a baseplate holder, and two alignment pieces. The waveguide comb contains many individual linear probes [Figs. 1(a) and 1(b)], each with optical waveguides running along its length, and each waveguide terminates at a different depth by a reflector that directs light [represented in Fig. 1(a) as blue cones] out of the side of the probe at that point. The design of the individual linear probes has been described previously [10]. The waveguide combs are produced by employing the same technology used to fabricate individual linear probes [10] but with a mask set patterned with arrays of probes, rather than individual probes. The SiON waveguides are fabricated on a silicon-on-insulator (SOI) wafer with device layer thickness of 50 μm, yielding a final probe thickness of 65 μm. The number of probes, the spacing of the probes, and the size and spacing of the output apertures are customizable depending on the brain regions targeted.

The baseplate holder is a single piece of 675 μm thick silicon with slots in which the waveguide combs sit perpendicularly [Figs. 1(a) and 1(b)]. For the purposes of accurate and uniform coupling, the waveguide combs must sit close to perpendicular in the baseplate holder and must be laterally spaced with a high degree of accuracy. Accordingly, 675 μm thick silicon alignment pieces were designed to accurately orient the waveguide combs, in both angle and lateral position, while avoiding probe

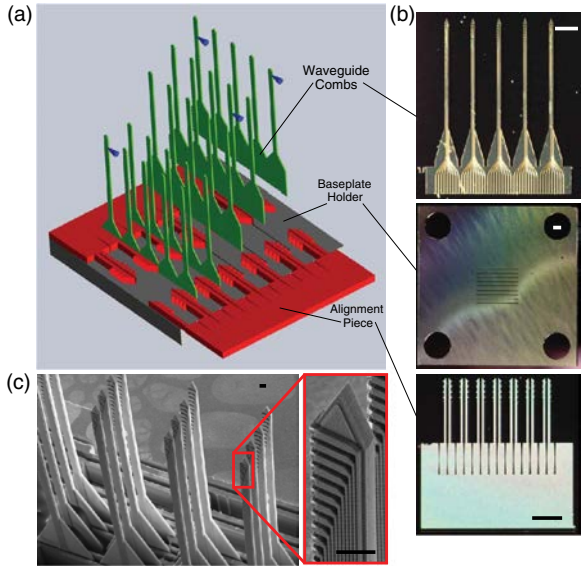

Fig. 1. (Color online) Design, fabrication, and assembly of an implantable 3D waveguide array capable of independent light delivery to sets of neural targets in brain tissue. (a) Schematic showing the assembly procedure. (b) Photomicrographs of waveguide comb, baseplate holder, and alignment piece. Scale bar, 1 mm. (c) SEM micrograph of assembled 3D waveguide array with a zoomed-in view of the output apertures. Output apertures shown here are 9 μm × 30 μm. Scale bar, 100 μm.

 © 2012 Optical Society of America

damage. The alignment piece geometry is a linear series of slots [Fig. 1(b)], which mechanically hold the waveguide combs in place. The contact between the alignment piece and the waveguide comb is in the lateral regions of the combs, which are free of any waveguides, and occurs along the vertical sidewall of the alignment slot (675 μm), thereby holding the comb vertical. By analyzing high-resolution images of assembled 1D probe arrays (combs), the angular deviation of the probes relative to the baseplate perpendicular direction was measured to be 0.9 ± 0.3 deg (mean $\pm$ standard deviation, $n = 10$ waveguide combs from two waveguide arrays). This small deviation appears to be due to a slight curvature of the probes, which translates to very small deviations (e.g., a 21 μm deviation of the tip position, for a 4-mm-long waveguide comb).

Both the baseplate holders and the alignment pieces are fabricated using a simple two-step silicon-dioxide hard mask and deep reactive-ion etch (DRIE) through-wafer etching. Then the 3D waveguide array is assembled by first inserting the combs into the baseplate holder, followed by two alignment pieces being pushed into place from either side. The series of sharp hooks at the tip of the alignment piece holds the alignment pieces together when inserted. The force between the alignment wedge and the waveguide combs keeps the two elements securely fastened. A UV-curable drop of epoxy is applied and exposed for permanent connection of all three elements. The device can be further coated (e.g., to insure long-term biocompatibility), although the current device is fine for acute to medium term experiments, as nonbiocompatible parts are external, and the device is sterilizable.

The waveguide comb fabrication process is performed on an SOI wafer with a device-layer thickness of 50 μm, buried oxide thickness of 2 μm, and handle thickness of 650 μm. A 3 μm layer of SiO_2 (index 1.46) is plasma-enhanced chemical vapor deposition (PECVD) deposited followed by a 9 μm layer of SiON (index 1.53). The waveguides are lithographically defined in a thick photoresist layer (AZ P4620) and the dielectric stack is etched through in a DRIE system. After removing all organics in a wet piranha etch and O_2 plasma, the hydrogen content in the SiON is dramatically lowered through an annealing step in a N_2 ambient at 1000°C for 3 h, critical for lowering Rayleigh-scattering losses in the waveguides. The 3 μm top cladding of SiO_2 (index 1.46) is then PECVD deposited. A 500 nm layer of Ti is sputtered over the entire probe, enabling the 90 deg corner mirror. The Ti layer is then selectively etched at the input and output aperture regions. A trench perimeter defining the final structure of the comb is defined lithographically in thick photoresist. Within that trench, the Ti layer and the 3 μm top cladding are wet-etched, leaving the silicon device layer exposed. The device layer is through-etched to the buried oxide layer using an SF6-based Bosch process. A backside through-etch to the buried oxide is then performed in a similar manner, yielding thin comb structures. The combs are released from the buried oxide frame holding the combs together in a hydrofluoric-vapor bath. Each individual waveguide has a measured propagation loss of 0.4 ± 0.1 dB/cm ($n = 10$) and a corner mirror loss of 1.5 ± 0.4 dB ($n = 4$), improved over our previous design [10] thanks to the choice of metal and the hydrogen elimination anneal.

A scanning electron micrograph of the final structure is shown in Fig. 1(c). When assembled, the waveguide inputs of the 3D system form a 2D array of apertures. A digital micromirror device (DMD) chipset provides a means of optically coupling a laser to the set of input apertures [Fig. 2(a)]. A laser beam is passed through a beam-shaper and zoom beam-expander to provide a flat-top circular illumination spatial profile to the DMD chip (Texas Instruments, 0.55 XGA DMD). The DMD chip's micromirrors (10 μm square, 10.8 μm pitch) reflect light at the correct angle for waveguide coupling for "on" pixels. The DMD image is projected onto a square microlens array (300 μm pitch, 8.7 mm focal length, Edmund Optics), each microlens of which collects 772 pixels and focuses the light onto an individual fiber of an image-bundle (Schott). The microlenses are necessary to attain the desired irradiance level at the waveguide output apertures. The image bundle is a densely packed array of fibers (8 μm core size, 10 μm pitch), where certain fibers are used to transfer the light collected by the microlens array to the 3D waveguide system, which is butt-coupled to the other end of the image bundle. By controlling sections of the DMD chipset as "on" or "off," it is possible to control which of the waveguides in the final 3D system are illuminated or not; a 1024×768 pixel DMD and 9.5 mm square image bundle, with 772 pixels per waveguide, would enable the control of

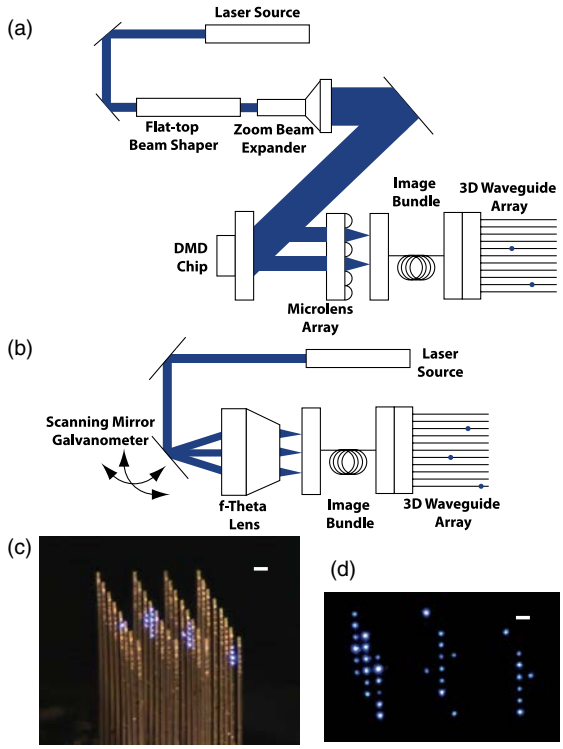

Fig. 2. (Color online) Optical systems for coupling light to 3D waveguide arrays. (a) Coupling method using a DMD chipset. (b) Coupling method using a scanning galvanometer. (c) Photomicrograph of 3D waveguide array showing an arbitrary illumination pattern using the DMD-based method. (d) Photomicrograph of the 3D waveguide array showing a DMD-mediated illumination pattern, "M-I-T". Scale bar, 150 μm.

up to ~1000 points in 3D space. The shown prototype 3D structure [Figs. 2(c) and 2(d)] has 192 output apertures. The total loss is found to be 17.3 ± 1.8 dB ($n = 15$ waveguides), measured with a photodiode sensor. One of the main sources of loss occurs at the DMD chipset: because it is composed of many individual reflecting micromirrors, the reflected light forms a diffraction pattern. Although the diffraction order with the highest energy [the (0,0) order] is used for coupling, the loss remains at 8.2 ± 0.3 dB ($n = 15$), caused by the remaining lost higher diffraction orders. Further contributing loss mechanisms include coupling losses at the image bundle-waveguide interface, including Fresnel losses and cross-sectional area mismatch. Depending on the waveguide comb pitch and the individual waveguide input pitch on each comb, the input apertures span a certain area of the baseplate holder, which must be covered by the DMD-shaped beam illumination. Given this broad area and the optical losses measured, a high-power laser source is necessary. For the shown prototype, a 1.5 W, 473 nm laser (Optoengine) was used and yielded an average maximum irradiance at the output aperture (9 μm thick, 60 μm wide) of 148 ± 56 mW/mm^2 ($n = 15$). Heating of the DMD chipset is negligible with sufficient cooling, as the reflection off of each micromirror is highly efficient.

An alternate coupling scheme is shown in Fig. 2(b). This method involves the use of a scanning galvanometer to direct the focused light of a laser beam to different regions of the image bundle. A telecentric f-theta lens focuses the light to a <9 μm spot size on the image bundle while mapping the changing angle of approach to a changing position in the image plane. The total loss is measured as 11.9 ± 2.5 dB ($n = 15$ waveguides). For the shown prototype, achieving an irradiance at the output aperture (9 μm thick, 60 μm wide) of 200 mW/mm^2 would require a source power of only 1.9 mW.

One of the DMD setup's strengths is its ability to illuminate sets of brain regions simultaneously, but the laser source must be powerful enough and the microlens elements large enough. For a given microlens element size and image bundle format size, an upper limit is placed on the number of waveguides possible. The galvanometer setup, in contrast, has no such limitation as the single source is, at any given time, responsible for illuminating a single region. The cost, however, is that it can be used only for scanning applications providing pulses of light sequentially from the illuminated ports.

A main source of loss in both coupling schemes is the interface between the image bundle and the 3D waveguide system (4.2 ± 1.7 dB, $n = 15$ waveguides). Because the two pieces are butt-coupled without any possibility of further alignment, and the manufacturing process for the image bundle yields a fiber lattice with positional nonuniformities, a large variance exists in the loss at this interface (hence the large standard deviations in total loss measured for both setups). The DMD and galvanometer setups, however, can both correct for this nonuniformity, to enable similar amounts of power to be delivered to different brain regions. The DMD setup correction involves adjusting the number of DMD pixels per waveguide, and the galvanometer setup correction involves adjusting the power supplied to each waveguide, empirically tuning these parameters with respect to a power measurement system.

We thank the MIT Microsystems Technology Laboratories for assistance and consultation on this project. CGF and ESB acknowledge support from the MIT McGovern Institute Neurotechnology Program, the Paul Allen Family Foundation, and the NIH grant NIH 1R01DA029639. ANZ acknowledges support from the McGovern Institute Hubert Schoemaker Fellowship, an NSF Graduate fellowship. ESB additionally acknowledges funding by the NSF CAREER Award CBET 1053233, the Human Frontiers Science Program MIT Media Lab, the Institution of Engineering and Technology A. F. Harvey Prize, and the New York Stem Cell Foundation Robertson Neuroscience Investigator Award.

References

1. E. S. Boyden, F. Zhang, E. Bamberg, G. Nagel, and K. Deisseroth, Nat. Neurosci. **8**, 1263 (2005).
2. X. Han and E. S. Boyden, PLoS ONE **2**, e299 (2007).
3. F. Zhang, L. P. Wang, M. Brauner, J. F. Liewald, K. Kay, N. Watzke, P. G. Wood, E. Bamberg, G. Nagel, A. Gottschalk, and K. Deisseroth, Nature **446**, 633 (2007).
4. B. Y. Chow, X. Han, A. S. Dobry, X. Qian, A. S. Chuong, M. Li, M. A. Henninger, G. M. Belfort, Y. Lin, P. E. Monahan, and E. S. Boyden, Nature **463**, 98 (2010).
5. X. Han, B. Y. Chow, H. Zhou, N. C. Klapoetke, A. Chuong, R. Rajimehr, A. Yang, M. V. Baratta, J. Winkle, R. Desimone, and E. S. Boyden, Front. Syst. Neurosci. **5**, 18 (2011).
6. T. V. F. Abaya, M. Diwekar, S. Blair, P. Tathireddy, L. Rieth, G. A. Clark, and F. Solzbacher, Proc. SPIE **8207**, 82075M (2012).
7. M. Im, I. J. Cho, F. Wu, K. D. Wise, and E. Yoon, *2011 IEEE 24th International Conference on Micro Electro Mechanical Systems* (IEEE, 2011), pp. 1051–1054.
8. S. Royer, B. V. Zemelman, M. Barbic, A. Losonczy, G. Buzsaki, and J. C. Magee, Eur. J. Neurosci. **31**, 2279 (2010).
9. E. Stark, T. Koos, and G. Buzsaki, J. Neurophysiol. **108**, 349 (2012).
10. A. N. Zorzos, E. S. Boyden, and C. G. Fonstad, Opt. Lett. **35**, 4133 (2010).